



Cite this: *J. Mater. Chem. C*, 2015, **3**, 10436

Synthesis, crystal structure, and transport properties of quaternary tetrahedral chalcogenides†

Yongkwan Dong,^a Lukasz Wojtas,^b Joshua Martin^c and George S. Nolas*^a

Quaternary chalcogenides with tetrahedral zinc-blend structure types continue to be of interest for thermoelectrics applications. We report on the synthesis, crystal structure, and high temperature transport properties of $\text{Cu}_{2.1}\text{Fe}_{0.9}\text{SnSe}_4$, $\text{Cu}_{2.2}\text{Fe}_{0.8}\text{SnSe}_4$ and $\text{Cu}_{2.2}\text{Zn}_{0.2}\text{Fe}_{0.6}\text{SnSe}_4$. The identity and compositions for each specimen were established using a combination of Rietveld refinement and elemental analysis and indicate that all compositions are homogeneous with the stannite crystal structure. Excess Cu reduces the electrical resistivity, ρ , by an order of magnitude compared with $\text{Cu}_2\text{FeSnSe}_4$ with no significant degradation of the Seebeck coefficient, S . The energy band gaps were estimated from the high temperature S values and indicate that $\text{Cu}_{2.1}\text{Fe}_{0.9}\text{SnSe}_4$ and $\text{Cu}_{2.2}\text{Fe}_{0.8}\text{SnSe}_4$ possess narrow band gaps, 0.18 eV and 0.25 eV, respectively, as compared to most other quaternary chalcogenides. The power factor ($\text{PF} = S^2/\rho$) increases with decreasing Fe content. Although $\text{Cu}_{2.2}\text{Fe}_{0.8}\text{SnSe}_4$ possesses a smaller PF than that of $\text{Cu}_{2.2}\text{Zn}_{0.2}\text{Fe}_{0.6}\text{SnSe}_4$, a ZT of 0.45 was obtained at 750 K for $\text{Cu}_{2.2}\text{Fe}_{0.8}\text{SnSe}_4$ due to its low thermal conductivity.

Received 2nd June 2015,
Accepted 9th July 2015

DOI: 10.1039/c5tc01606a

www.rsc.org/MaterialsC

Introduction

Thermoelectric devices are of interest for waste heat recovery and solid-state cooling applications.¹ The measure of thermoelectric materials is governed by their dimensionless figure-of-merit ZT ($=S^2T/\rho\kappa$, where S is the Seebeck coefficient, T is the absolute temperature, ρ the electrical resistivity, and κ the thermal conductivity which is typically defined as the sum of the lattice thermal conductivity, κ_L , and the electronic contribution, κ_E) in the temperature range of interest. It is however challenging to optimize ZT since these three parameters (S , ρ , and κ) are dependent on each other.^{1–4} Recent research on the thermoelectric properties of existing or new materials, and their synthesis and subsequent optimization, have focused on an understanding of their structure–property relationships.

Tetrahedral quaternary chalcogenides, such as Cu_2MSnQ_4 (M = transition metals with a +2 oxidation state, and Q = S, Se, Te) made up of earth-abundant elements, continue to be of interest due to their diversity of applications, including solar-cell absorbers,⁵ photocatalysts for solar water splitting,⁶ nonlinear optics,⁷ topological insulators,⁸ magneto-optic and magneto-ferroics,⁹ and thermoelectrics.¹⁰ Certain quaternary chalcogenides, such as

$\text{Cu}_2\text{ZnSnSe}_4$ and $\text{Cu}_2\text{CdSnSe}_4$,¹⁰ have been studied as potential thermoelectric materials for power generation applications due to their inherently low κ induced by their structural features. These materials possess relatively wide band gaps, which is not typical of thermoelectric materials,⁴ however their transport properties can be varied by appropriate doping and/or variations in stoichiometry. Nano-scale effects on the thermoelectric properties have also been investigated.¹¹ Further reduction of κ is feasible by alloying where point defect scattering induced by local anisotropic structural disorder leads to a reduction in κ_L .^{10,11–20}

Certain quaternary chalcogenide compositions have been shown to exhibit relatively good ZT values at high temperature. Nevertheless the ρ values are relatively high as compared with that of state-of-the-art thermoelectric materials.³ Herein we report on the synthesis, crystal structure, and electrical and thermal transport properties of the modified quaternary chalcogenides $\text{Cu}_{2.1}\text{Fe}_{0.9}\text{SnSe}_4$, $\text{Cu}_{2.2}\text{Fe}_{0.8}\text{SnSe}_4$ and $\text{Cu}_{2.2}\text{Zn}_{0.2}\text{Fe}_{0.6}\text{SnSe}_4$. We investigated alloying of the quaternary compositions while maintaining a higher than stoichiometric Cu content since excess Cu has been shown to enhance the thermoelectric properties of these materials.^{10,17}

Experimental

Synthesis

Polycrystalline bulk specimens were prepared by the direct reaction of the constituent elements. Cu powder (99.9%, Alfa Aesar), Fe

^a Department of Physics, University of South Florida, Tampa, FL 33620, USA.

E-mail: gnolas@usf.edu

^b Department of Chemistry, University of South Florida, Tampa, FL 33620, USA

^c Material Measurement Laboratory, National Institute of Standards and Technology, Gaithersburg, MD 20899, USA

† Electronic supplementary information (ESI) available. See DOI: 10.1039/c5tc01606a

powder (99.998%, Alfa Aesar), Zn shot (99.9999%, Alfa Aesar), Sn powder (99.999%, Alfa Aesar), and Se powder (99.999%, Alfa Aesar) were loaded into silica ampoules in stoichiometric ratios $\text{Cu}_{2+x}\text{Fe}_{1-x}\text{SnSe}_4$ (where $x = 0.1$ and 0.2) and $\text{Cu}_{2.2}\text{Zn}_{0.2}\text{Fe}_{0.6}\text{SnSe}_4$.²¹ The reaction ampoules were sealed in quartz tubes under vacuum, heated to 1023 K and subsequently held at this temperature for 5 d. The furnace was turned off and the reaction tubes were quenched to room temperature in air. The products were ground into fine powders and sieved (≈ 325 mesh) inside a glovebox before being loaded into graphite dies for hot pressing. Densification was accomplished by hot pressing at 873 K and 150 MPa for 3 h under N_2 flow. The density of the hot-pressed pellets was determined by measurement of their dimensions and weight after polishing the surfaces of the pellets. These measurements indicated that high density polycrystalline specimens ($>95\%$ of theoretical density) were obtained.

Physical characterization

Powder X-ray diffraction (PXRD) and energy-dispersive X-ray spectroscopy (EDS) were used to examine the purity and chemical composition of the specimens. PXRD data were collected with a Bruker D8 Advance diffractometer with DAVINCI design equipped with a Lynxeye detector using $\text{Cu K}\alpha$ radiation and examined by the Rietveld method using a TOPAS 4.2.²² EDS of the hot-pressed pellets was accomplished with an Oxford INCA X-Sight 7582M equipped scanning electron microscope (SEM, JEOL JSM-6390LV). The average atomic ratios were calculated from at least twelve data sets obtained from random positions of the hot pressed pellet for each specimen. Optical diffuse reflectance measurements were performed at room temperature using a JASCO V-670 UV-Vis double beam Spectrophotometer equipped with a 60 mm diameter integrating sphere. A fine powder for each specimen was prepared by grinding the polycrystalline specimen that was then compacted between two quartz slides. Reflectance data were collected in the wavelength range of 200–2700 nm.

High temperature S and ρ were measured on parallelepipeds ($2\text{ mm} \times 2\text{ mm} \times 10\text{ mm}$), cut from the hot pressed pellets, with a custom-designed and constructed apparatus at NIST (2σ expanded uncertainty of 1.5%, and 1.2% for S and ρ , respectively).²³ High temperature κ values were determined using the equation $\kappa = D \cdot \alpha \cdot C_p$ where D is the measured density from geometry, α is the measured thermal diffusivity, and C_p is the specific heat. Thermal diffusivity measurements employed the laser flash method in a flowing He environment with a NETZSCH LFA 457 system. The uncertainty in the thermal diffusivity measurements were $\approx 5\%$. Heat capacity C_p ($\approx C_v$) was estimated with the Dulong–Petit limit ($C_v = 3nR$, where n is the number of atoms per formula unit and R is the ideal gas constant). At high temperature this may sometimes result in an underestimation of C_p , thus affecting κ , however it is a relatively good method for comparing the effect of doping and compositional changes since it eliminates the uncertainties associated with C_p measurements.²⁴ The S and ρ measurements were performed perpendicular to the pressing axis, whereas the laser flash diffusivity measurements were carried out on the entire pellet parallel to the pressing axis.

Results and discussion

PXRD results revealed all specimens to be single phase with the tetragonal crystal structure with no change before and after hot pressing. All reflections for all three compositions can be indexed to $\text{Cu}_2\text{FeSnSe}_4$ ²⁵ with no secondary phases. The initial positional parameters for all the atoms in the structure were from data on $\text{Cu}_2\text{FeSnSe}_4$. The space group $I\bar{4}2m$ (#121) was applied to refine the crystal structure. The excess Cu or Zn substitution are located at the crystallographic $2a$ site along with Fe. Site occupancy refinements of each atom for each composition were carried out to check for any structural disorder. For all compositions each crystallographic site is fully occupied. The atomic coordinates and displacement parameters were refined and the final values obtained were with full least-square refinements. The observed and calculated PXRD patterns and the difference profiles for each specimen are given in Fig. 1. Detailed refinement results are shown in Table 1. Fig. 1(d) shows the crystal structure of $\text{Cu}_{2.2}\text{Fe}_{0.8}\text{SnSe}_4$ based on our refinement results as representative of all three specimens. The crystal structure is composed of two different metal–selenium, $[\text{Cu}_2\text{Se}_2]$ and $[\text{MSnSe}_2]$ ($M = \text{Cu/Fe}$ or Cu/Zn/Fe), layers with an alternative stacking along the crystallographic c axis. Each $[\text{MSnSe}_2]$ layer is translated relative to each other by $\bar{4}$ symmetry along the crystallographic a axis in between $[\text{Cu}_2\text{Se}_2]$ layers. All metal atoms are surrounded by four Se atoms in a tetrahedral geometry and the Se atoms are also tetrahedrally bounded by four metal atoms (two Cu1, one M (Cu/Fe or Cu/Zn/Fe), and one Sn). Metal–Se bond distances range from 2.422 (1) Å to 2.441 (1) Å for Cu1, 2.402 (2) Å to 2.433 (2) Å for M, and 2.557 (2) Å to 2.560 (2) Å for Sn and average angles are very close to the ideal tetrahedral angle.^{15–17,25} Fig. 2 shows SEM images and EDS elemental mapping images of hot pressed $\text{Cu}_{2.2}\text{Fe}_{0.8}\text{SnSe}_4$ as representative of our analyses. Fig. 2(a) and (b) indicate no texturing in the specimen and EDS analyses revealed that each element was uniformly distributed. The compositions obtained from our refinements are consistent with those obtained from elemental analyses.

Fig. 3(a) and (b) show temperature dependent ρ and S values, respectively, for all compositions. The ρ values for all compositions are an order of magnitude lower as compared with that of other stoichiometric compounds.^{10,11,14,17} While ρ of $\text{Cu}_{2.1}\text{Fe}_{0.9}\text{SnSe}_4$ increases with increasing temperature, ρ of $\text{Cu}_{2.2}\text{Fe}_{0.8}\text{SnSe}_4$ and $\text{Cu}_{2.2}\text{Zn}_{0.2}\text{Fe}_{0.6}\text{SnSe}_4$ decreases with increasing temperature. The S values of $\text{Cu}_{2.1}\text{Fe}_{0.9}\text{SnSe}_4$ and $\text{Cu}_{2.2}\text{Fe}_{0.8}\text{SnSe}_4$ increase with increasing temperature and reach a maximum at 690 K and 440 K, respectively, corresponding to a change of the slope in ρ . This is presumably due to a phase transition¹¹ as well as thermal excitation of minority carriers. For $\text{Cu}_{2.2}\text{Zn}_{0.2}\text{Fe}_{0.6}\text{SnSe}_4$ S increases steadily with increasing temperature. Our results indicate that ρ can be tuned without significant reduction in S by incorporating excess Cu.

UV/Vis diffuse reflectance spectroscopy measurements were performed for all three specimens however the spectra did not show any edge over the entire measurement range (2700 nm to 200 nm; 0.46 eV to 6.22 eV). This indicates that these compounds

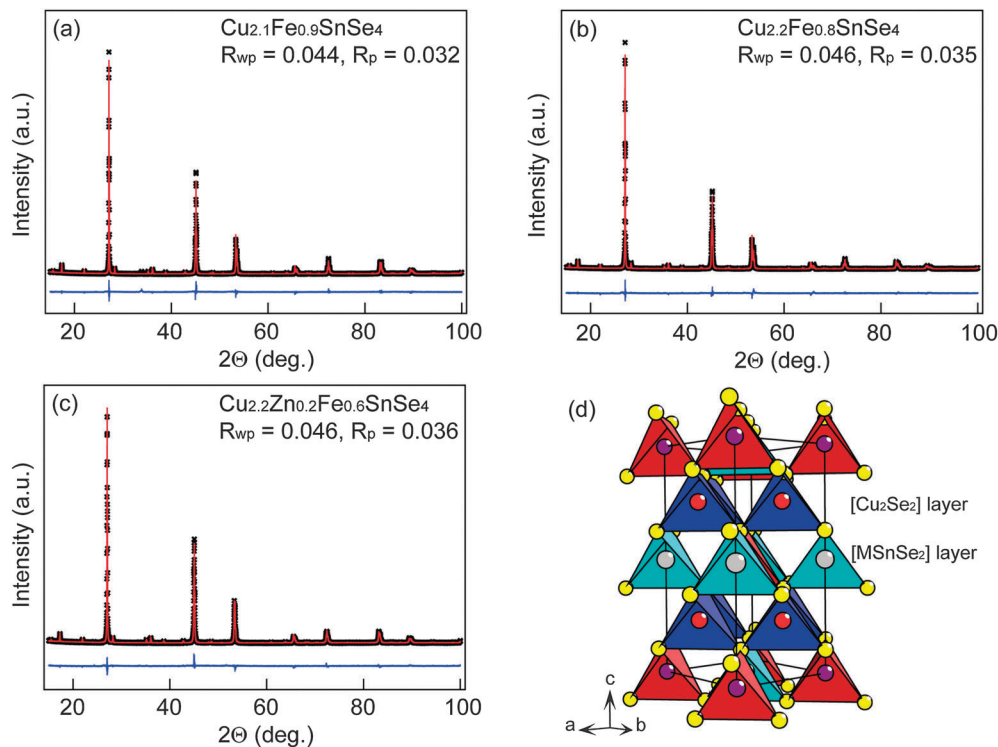


Fig. 1 PXRD data for (a) $\text{Cu}_{2.1}\text{Fe}_{0.9}\text{SnSe}_4$, (b) $\text{Cu}_{2.2}\text{Fe}_{0.8}\text{SnSe}_4$, (c) $\text{Cu}_{2.2}\text{Zn}_{0.2}\text{Fe}_{0.6}\text{SnSe}_4$ including profile fit (black cross mark), profile difference (red line), and profile residuals (blue line) from Rietveld refinement, and (d) crystal structure composed of two $[\text{Cu}_2\text{Se}_2]$ and $[\text{MSnSe}_2]$ layers. Red circle is Cu (4d; 0, 0.5, 0.25), purple circle is M (mixed 2a; 0, 0, 0), gray circle is Sn (2b; 0, 0, 0.5), and yellow circle is Se (8i; x, x, z).

Table 1 Lattice parameters, Se atomic coordinates, selected bond distances (Å) and angles (deg.) for $\text{Cu}_{2.1}\text{Fe}_{0.9}\text{SnSe}_4$, $\text{Cu}_{2.2}\text{Fe}_{0.8}\text{SnSe}_4$, and $\text{Cu}_{2.2}\text{Zn}_{0.2}\text{Fe}_{0.6}\text{SnSe}_4$

Composition	$\text{Cu}_{2.1}\text{Fe}_{0.9}\text{SnSe}_4$	$\text{Cu}_{2.2}\text{Fe}_{0.8}\text{SnSe}_4$	$\text{Cu}_{2.2}\text{Zn}_{0.2}\text{Fe}_{0.6}\text{SnSe}_4$
EDS	$\text{Cu}_{2.10(7)}\text{Fe}_{0.84(3)}\text{Sn}_{0.94(2)}\text{Se}_{3.95(8)}$	$\text{Cu}_{2.20(4)}\text{Fe}_{0.75(2)}\text{Sn}_{0.95(2)}\text{Se}_{3.94(5)}$	$\text{Cu}_{2.20(4)}\text{Zn}_{0.22(2)}\text{Fe}_{0.55(3)}\text{Sn}_{0.91(2)}\text{Se}_{4.05(4)}$
Space group, Z	$I\bar{4}2m$ (#121), 2		
a, Å	5.6898 (1)	5.6927 (1)	5.6825 (1)
c, Å	11.3197 (1)	11.2981 (1)	11.3238 (1)
V, Å ³	366.46 (1)	366.14 (1)	365.65 (1)
Radiation	Cu K α (1.54056 Å)		
$D_{\text{calc.}}$, g cm ⁻³	5.60	5.61	5.67
GOF	2.00	1.61	1.55
Se, x and z	0.2397 (2), 0.1298 (3)	0.2381 (2), 0.1281 (2)	0.2401 (2), 0.1308 (2)
Cu1–Se	2.430 (2)	2.441 (1)	2.422 (1)
M–Se ^a	2.425 (2)	2.402 (2)	2.433 (2)
Sn–Se	2.558 (2)	2.557 (2)	2.560 (2)
Se–Cu1–Se	108.3 (1), 111.9 (1)	108.6 (1), 111.3 (1)	108.1 (1), 112.2 (1)
Se–M–Se	105.4 (1), 111.5 (1)	105.9 (1), 111.3 (1)	105.0 (1), 111.8 (1)
Se–Sn–Se	109.3 (1), 109.9 (1)	108.7 (1), 111.1 (1)	109.3 (1), 109.6 (1)

^a M is Cu_2/Fe or $\text{Cu}_2/\text{Zn}/\text{Fe}$.

possess band gaps below 0.46 eV. We therefore estimated the band gap of these compounds from the temperature dependent S data. The energy gap, E_g , can be estimated from the equation $S_{\text{max}} \approx E_g/2eT_{\text{max}}$ where e is the elementary charge and T_{max} is the absolute temperature at the highest S value, S_{max} .²⁶ Employing this formulation, E_g values of 0.25 eV for $\text{Cu}_{2.1}\text{Fe}_{0.9}\text{SnSe}_4$ and 0.18 eV for $\text{Cu}_{2.2}\text{Fe}_{0.8}\text{SnSe}_4$ are obtained, respectively. This result indicates that band gap tuning may be possible by changing the Cu content without significant degradation of S , and may indicate another potential optimization route for these materials.

The temperature dependence of the high temperature κ and estimated κ_L values are shown in Fig. 4(a) and (b), respectively. Both κ and κ_L decrease gradually with increasing temperature. The κ_L values (Fig. 4(b)) were estimated using $\kappa_L = \kappa - \kappa_E$ and the Wiedemann–Franz relation where $\kappa_E = L_0\sigma T$, and σ is the electrical conductivity, $\sigma = 1/\rho$. Kim *et al.*²⁷ proposed the equation $L = 1.5 + \exp(-|S|/116)$, where L is in $10^{-8} \text{ V}^2 \text{ K}^{-2}$ and S is in $\mu\text{V K}^{-1}$, to estimate the Lorenz number for the single parabolic band and acoustic phonon scattering approximations. Using this equation and data from Fig. 3(a) and (b) we

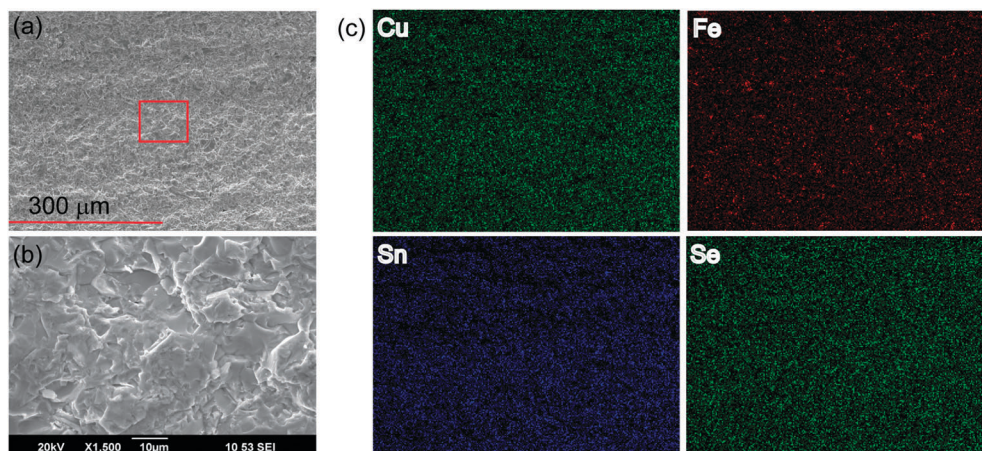


Fig. 2 (a) SEM image of a cross section, (b) magnified SEM image of the area represented by a red square in (a), and (c) EDX elemental mapping images of SEM image (a) for hot-pressed $\text{Cu}_{2.2}\text{Fe}_{0.8}\text{SnSe}_4$.

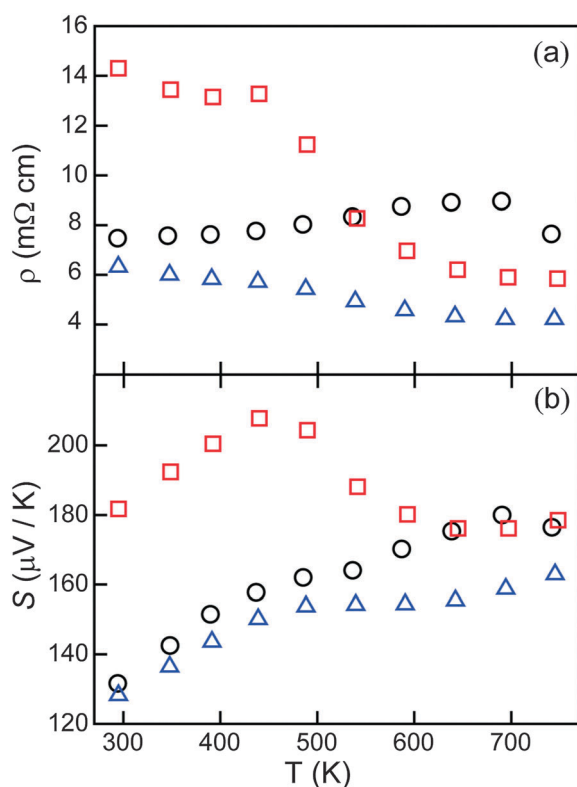


Fig. 3 Temperature dependent (a) ρ and (b) S data for $\text{Cu}_{2.1}\text{Fe}_{0.9}\text{SnSe}_4$ (○), $\text{Cu}_{2.2}\text{Fe}_{0.8}\text{SnSe}_4$ (□), and $\text{Cu}_{2.2}\text{Zn}_{0.2}\text{Fe}_{0.6}\text{SnSe}_4$ (△).

estimated κ_{B} , nevertheless κ_{L} is the dominant contribution at room temperature ($\approx 97\%$ of κ) and at the highest temperatures of our measurements ($\approx 75\%$ of κ). The temperature dependence of κ_{L} is proportional to T^{-1} over the entire measurement range thus the contribution to κ by bipolar diffusion, κ_{B} , can be estimated from the data at elevated temperatures (see inset in Fig. 4(b)). Here κ_{B} is the difference between the fit line and κ_{L} at the highest measured temperatures. At 750 K the portion of κ_{B} is about 9% of κ for $\text{Cu}_{2.1}\text{Fe}_{0.9}\text{SnSe}_4$

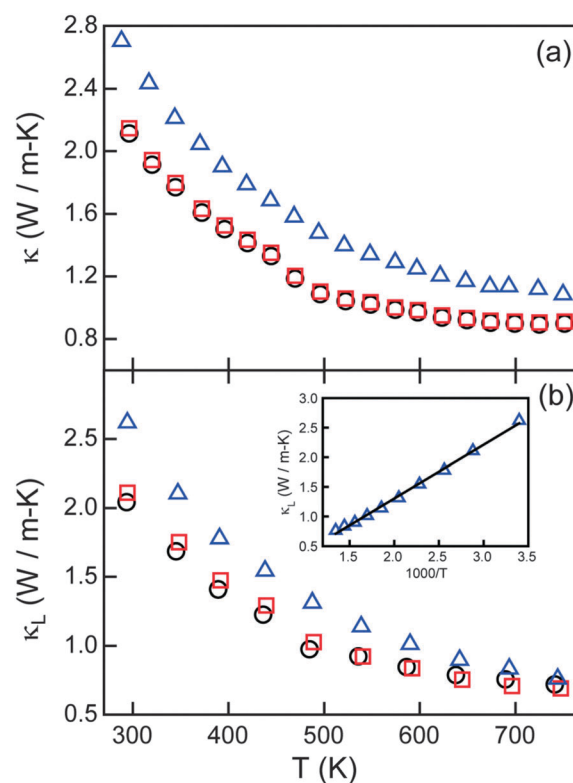


Fig. 4 Temperature dependent (a) κ and (b) κ_{L} for $\text{Cu}_{2.1}\text{Fe}_{0.9}\text{SnSe}_4$, $\text{Cu}_{2.2}\text{Fe}_{0.8}\text{SnSe}_4$, and $\text{Cu}_{2.2}\text{Zn}_{0.2}\text{Fe}_{0.6}\text{SnSe}_4$. The solid line in the inset shows the T^{-1} dependence of κ_{L} for $\text{Cu}_{2.2}\text{Zn}_{0.2}\text{Fe}_{0.6}\text{SnSe}_4$. The symbols corresponding to each specimen are as defined in Fig. 3.

and $\text{Cu}_{2.2}\text{Fe}_{0.8}\text{SnSe}_4$, and 5% for $\text{Cu}_{2.2}\text{Zn}_{0.2}\text{Fe}_{0.6}\text{SnSe}_4$. It is likely that κ_{B} increases with increasing temperature due to excitation of minority carrier. This also agrees with the S data which shows a peak, or deviation, in slope at higher temperatures.

The calculated ZT and the power factor ($\text{PF} = S^2/\rho$) values using the data in Fig. 3 and 4 for all compositions are shown in Fig. 5. The PF values increase with increasing temperature and

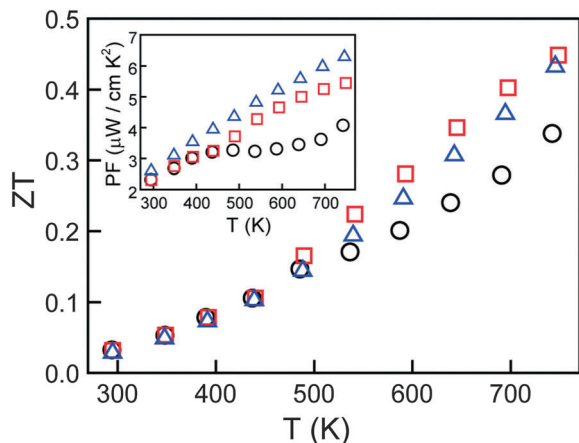


Fig. 5 ZT and PF (inset) as a function of temperature for $\text{Cu}_{2.1}\text{Fe}_{0.9}\text{SnSe}_4$, $\text{Cu}_{2.2}\text{Fe}_{0.8}\text{SnSe}_4$, and $\text{Cu}_{2.2}\text{Zn}_{0.2}\text{Fe}_{0.6}\text{SnSe}_4$. The symbols corresponding to each specimen are as defined in Fig. 3.

decreasing Fe content. The highest PF is $6.3 \mu\text{W cm}^{-1} \text{K}^{-2}$ for $\text{Cu}_{2.2}\text{Zn}_{0.2}\text{Fe}_{0.6}\text{SnSe}_4$, and is comparable with that of nanostructured $\text{Cu}_{2+x}\text{Zn}_{1-x}\text{GeSe}_4$ solid solutions.¹¹ For all compositions, the ZT values increase rapidly with increasing temperature. The highest ZT value (0.45) was obtained at 750 K for $\text{Cu}_{2.2}\text{Fe}_{0.8}\text{SnSe}_4$ due to a low κ , although the PF values are lower than that of $\text{Cu}_{2.2}\text{Zn}_{0.2}\text{Fe}_{0.6}\text{SnSe}_4$ which also has a relatively high ZT due to low ρ values. These results represent another avenue for thermoelectric properties enhancements in these materials.

Conclusion

Polycrystalline Cu excess modified zinc-blend tetrahedral quaternary chalcogenides, $\text{Cu}_{2.1}\text{Fe}_{0.9}\text{SnSe}_4$, $\text{Cu}_{2.2}\text{Fe}_{0.8}\text{SnSe}_4$ and $\text{Cu}_{2.2}\text{Zn}_{0.2}\text{Fe}_{0.6}\text{SnSe}_4$, were synthesized and their structural and high temperature transport properties were investigated. Rietveld refinement and elemental analyses confirm the composition of each specimen to be close to that of their nominal compositions while all compositions are homogeneous without any secondary phases. The estimated band gaps, from high temperature S values, indicate that all specimens possess relatively narrow band gaps, between 0.18 eV and 0.25 eV, as compared to most other similar compositions. The PF increases with increasing substitution on the Fe site. A ZT value of 0.45 was obtained at 750 K for $\text{Cu}_{2.2}\text{Fe}_{0.8}\text{SnSe}_4$, the specimen with high S and low κ , and is higher than that of $\text{Cu}_2\text{Zn}_{0.4}\text{Fe}_{0.6}\text{SnSe}_4$ (≈ 0.4 at 750 K)¹⁵ and $\text{Cu}_2\text{Zn}_{0.1}\text{Fe}_{0.9}\text{GeSe}_4$ (≈ 0.2 at 650 K).¹⁴

Acknowledgements

This work was supported by the National Science Foundation Grant No. DMR-1400957. We thank Dr J. R. Salvador at GM for diffusivity measurements.

References

- 1 T. M. Tritt, *Annu. Rev. Mater. Res.*, 2011, **41**, 433–448.
- 2 F. J. DiSalvo, *Science*, 1999, **285**, 703–706.
- 3 G. S. Nolas, J. W. Sharp and H. J. Goldsmid, *Thermoelectrics: Basics Principles and New Materials Developments*, Springer-Verlag, 2001.
- 4 G. D. Mahan, *Solid State Phys.*, 1998, **51**, 81–157.
- 5 K. Tanaka, M. Oonuki, N. Moritake and H. Uchiki, *Sol. Energy Mater. Sol. Cells*, 2009, **93**, 583–587; Q. Guo, G. M. Ford, W. C. Yang, B. C. Walker, E. A. Stach, H. W. Hillhouse and R. Agrawal, *J. Am. Chem. Soc.*, 2010, **132**, 17384–17386.
- 6 I. Tsuji, Y. Shimodaira, H. Kato, H. Kobayashi and A. Kudo, *Chem. Mater.*, 2010, **22**, 1402–1409.
- 7 L. K. Samanta and G. C. Bhar, *Phys. Status Solidi A*, 1977, **41**, 331–337.
- 8 S. Chen, X. G. Gong, C.-G. Duan, Z.-Q. Zhu, J.-H. Chu, A. Walsh, Y. G. Yao, J. Ma and S.-H. Wei, *Phys. Rev. B: Condens. Matter Mater. Phys.*, 2011, **83**, 245202.
- 9 T. Fries, Y. Shapira, F. Palacio, M. C. Moron, G. J. McIntyre, R. Kershaw, A. Wold and E. J. McNiff, *Phys. Rev. B: Condens. Matter Mater. Phys.*, 1997, **56**, 5424–5431; G. Nenert and T. T. M. Palstra, *J. Phys.: Condens. Matter*, 2009, **21**, 176002.
- 10 M. L. Liu, F. Q. Huang, L. D. Chen and I. W. Chen, *Appl. Phys. Lett.*, 2009, **94**, 202103; M. L. Liu, I. W. Chen, F. Q. Huang and L. D. Chen, *Adv. Mater.*, 2009, **21**, 3808–3812.
- 11 M. Ibáñez, D. Cadavid, R. Zamani, N. García-Castelló, V. Izquierdo-Roca, W. Li, A. Fairbrother, J. D. Prades, A. Shavel, J. Arbiol, A. Pérez-Rodríguez, J. R. Morante and A. Cabot, *Chem. Mater.*, 2012, **24**, 562–570; M. Ibáñez, R. Zamani, A. LaLonde, D. Cadavid, W. Li, A. Shavel, J. Arbiol, J. R. Morante, S. Gorsse, G. J. Snyder and A. Cabot, *J. Am. Chem. Soc.*, 2012, **134**, 4060–4063; W. G. Zeier, A. LaLonde, Z. M. Gibbs, C. P. Heinrich, M. Panthöfer, G. J. Snyder and W. Tremel, *J. Am. Chem. Soc.*, 2012, **134**, 7147–7154.
- 12 X. Y. Shi, F. Q. Huang, M. L. Liu and L. D. Chen, *Appl. Phys. Lett.*, 2009, **94**, 122103.
- 13 Ch. Raju, M. Falmbigl, P. Rogl, X. Yan, E. Bauer, J. Horiky, M. Zehetbauer and R. C. Mallik, *AIP Adv.*, 2013, **3**, 032106.
- 14 W. G. Zeier, Y. Pei, G. Pomrehn, T. Day, N. Heinz, C. P. Heinrich, G. J. Snyder and W. Tremel, *J. Am. Chem. Soc.*, 2013, **135**, 726–732.
- 15 Y. Dong, H. Wang and G. S. Nolas, *Inorg. Chem.*, 2013, **52**, 14364–14367.
- 16 C. P. Heinrich, T. W. Day, W. G. Zeier, G. J. Snyder and W. Tremel, *J. Am. Chem. Soc.*, 2014, **136**, 442–448.
- 17 Y. Dong, H. Wang and G. S. Nolas, *Phys. Status Solidi RRL*, 2014, **8**, 61–64.
- 18 J. Navrátil, V. Kucek, T. Plecháček, E. Černošková, F. Laufek, Č. Drašar and P. Kmotek, *J. Electron. Mater.*, 2014, **43**, 3719–3725.
- 19 R. Chetty, J. Dadda, J. de Boer, E. Müller and R. C. Mallik, *Intermetallics*, 2015, **57**, 156–162.
- 20 Y. Dong, B. Eckert, H. Wang, X. Zeng, T. M. Tritt and G. S. Nolas, *Dalton Trans.*, 2015, **44**, 9014–9019.
- 21 Certain commercial equipment, instruments, or materials are identified in this document. Such identification neither does

- imply recommendation or endorsement by the National Institute of Standards and Technology nor does it imply that the products identified are necessarily the best available for the purpose.
- 22 TOPAS V4 general profile and structure analysis software for powder diffraction data, Bruker AXS, Karlsruhe, Germany.
- 23 J. Martin, *Rev. Sci. Instrum.*, 2012, **83**, 065101.
- 24 H. Wang, W. D. Porter, H. Bottner, J. Kronig, L. Chen, S. Bai, T. M. Tritt, A. Mayolet, J. Senawiratne, C. Smith, F. Harris, P. Gillbert, J. Sharp, J. Lo, H. Kleinke and L. Kiss, *J. Electron. Mater.*, 2013, **42**, 1073–1084.
- 25 E. Roque Infante, J. M. Delgado and S. A. López Rivera, *Mater. Lett.*, 1997, **33**, 67–70.
- 26 H. J. Goldsmid and J. W. Sharp, *J. Electron. Mater.*, 1999, **28**, 869–872.
- 27 H.-S. Kim, Z. M. Gibbs, Y. Tang, H. Wang and G. J. Snyder, *APL Mater.*, 2015, **3**, 041506.